JOURNAL OF MATERIALS SCIENCE 28 (1993) 2750–2756

Prediction of creep deformation in ductile two-phase alloys by a continuum mechanics model

M. TANAKA
Department of Mechanical Engineering, Mining College, Akita University, 1-1, Tegatagakuen-cho, Akita 010, Japan

The creep deformation of the ductile two-phase alloys was analysed on the basis of the continuum mechanics model which incorporated the Θ projection concept proposed by Evans and Wilshire. The calculated creep curves were compared with the experimental ones in ferrite–pearlite steels. It was found that the continuum mechanics model was able to predict the whole creep deformation process of the ductile two-phase alloys from the onset of creep loading to the final rupture, if the creep–deformation and creep–rupture data of the individual phases which constituted the two-phase alloys were known. A "steady-state creep" in the ductile two-phase alloys was predicted by the continuum mechanics model to occur, even if the constituent phases did not have the inherent steady-state creep. This was caused by the internal stresses arising from the creep–strength difference between second-phase and matrix in the two-phase alloys. This steady-state creep was observed in ferrite–pearlite steels during creep at 873 K. The predicted rupture life on the basis of the continuum mechanics model was correlated well with the experimental results in ferrite–pearlite steels, although the former was somewhat shorter than the latter under higher creep stresses. The continuum mechanics model was able to apply to the life prediction and the creep–strength design of the ductile two-phase alloys.

1. Introduction

Various kinds of constitutive equations which describe the creep deformation (creep curve) of metallic materials have been proposed by many investigators [1–4]. However, the constitutive equation which can simulate the whole creep curve from the onset of creep loading to the final rupture has not been known until recently. The Θ projection concept proposed by Evans and Wilshire [5] is a successful method which reasonably describes the whole creep curve of materials, and is applied to the interpolation and extrapolation of creep deformation from existing creep data in metallic and non-metallic materials [5, 6].

It was shown in the previous study that creep deformation in a ductile two-phase alloy can be predicted to some extent on the basis of the continuum mechanics model from the stress dependence of the steady-state creep rate of the constituent phases [7]. The continuum mechanics model is capable of incorporating any creep law, and is therefore applicable to the prediction of the whole creep deformation process in ductile two-phase alloys, if creep data of these two phases are obtained.

In this study, the continuum mechanics model which incorporates the Θ projection concept was applied to the prediction of the whole creep deformation process in ductile two-phase alloys. The results of the calculations based on the model were compared with the experimental results on the ferrite–pearlite steels crept at 873 K. The rupture life of the two-phase alloys was also predicted on the basis of the continuum mechanics model.

2. Continuum mechanics model

2.1. Stresses and creep strains

The basic equations of stresses and creep strains in this study are the same as those shown in the previous paper [7]. Let us consider the creep deformation of a ductile two-phase alloy, in which the second-phase particles with an arbitrary shape and volume fraction, f, are dispersed in the matrix phase [7]. It is assumed in this study that both phases are elastically and plastically isotropic, and that creep strains are uniform in individual phases ($\varepsilon^{I}_{33} = -2\varepsilon^{I}_{11} = -2\varepsilon^{I}_{22}$ for the matrix (phase I) and $\varepsilon^{II}_{33} = -2\varepsilon^{II}_{11} = -2\varepsilon^{II}_{22}$ for the second phase (phase II) under an applied tensile stress, σ^{A}_{33}). Components of creep strain difference between two phases are $\Delta\varepsilon_{33}$ ($= \varepsilon^{I}_{33} - \varepsilon^{II}_{33}$), $\Delta\varepsilon_{11}$ ($= \varepsilon^{I}_{11} - \varepsilon^{II}_{11}$), and $\Delta\varepsilon_{22}$ ($= \varepsilon^{I}_{22} - \varepsilon^{II}_{22} = \Delta\varepsilon_{11}$). Internal stresses arise from the strain difference, $\Delta\varepsilon_{ij}$. The components of internal stresses averaged over the matrix, σ^{I}_{ij}, and these for the second phase, σ^{II}_{ij}, can be calculated by the equivalent inclusion method [8–11] and the average internal stress concept [12], and are

0022–2461

expressed as

$$\sigma^{I}_{33} = -fAE\Delta\varepsilon_{33} = -fAEx \quad (1a)$$

$$\sigma^{I}_{11} = \sigma^{I}_{22} = fBE\Delta\varepsilon_{33} = fBEx \quad (1b)$$

$$\sigma^{II}_{33} = (1-f)AE \quad (2a)$$

$$\sigma^{II}_{11} = \sigma^{II}_{22} = -(1-f)BEx \quad (2b)$$

where x is $\Delta\varepsilon_{33}$ and E is Young's modulus ($E = 2\mu \times (1+\nu)$, μ = rigidity; ν = Poisson's ratio). A and B are functions of Eshelby's tensor [8–11], elastic moduli of the matrix phase (E, μ and ν) and those of the second phase (E^*, μ^* and ν^*). The actual stresses, the equivalent stress of von Mises type, σ_e, and the deviatoric stress, σ'_{ij}, are

$$\sigma^{A}_{33} + \sigma^{I}_{33} = \sigma^{A}_{33} - fAEx \quad (3a)$$

$$\sigma^{I}_{22} = \sigma^{I}_{11} = fBEx \quad (3b)$$

$$\sigma^{I}_{e} = \sigma^{A}_{33} - f(A+B)Ex = \sigma^{A}_{33} - fKEx \quad (3c)$$

$$\sigma'^{I}_{33} = -2\sigma'^{I}_{22} = -2\sigma'^{I}_{11} = (2/3)(\sigma^{A}_{33} - fKEx) \quad (3d)$$

for the matrix, and

$$\sigma^{A}_{33} + \sigma^{II}_{33} = \sigma^{A}_{33} + (1-f)AEx \quad (4a)$$

$$\sigma^{II}_{22} = \sigma^{II}_{11} = -(1-f)BEx \quad (4b)$$

$$\sigma^{II}_{e} = \sigma^{A}_{33} + (1-f)KEx \quad (4c)$$

$$\sigma'^{II}_{33} = -2\sigma'^{II}_{22} = -2\sigma'^{II}_{11} = (2/3)[\sigma'^{A}_{33} + (1-f)KEx] \quad (4d)$$

for the second phase, where K ($= A + B$) is a shape factor [7]. The value of shape factor K is $(7-5\nu)/[10(1-\nu^2)]$ for the spherical second phase of the same elastic moduli as those of the matrix [8]. The average creep strain of the two-phase alloy, ε_{ij}, is expressed as

$$\varepsilon_{ij} = (1-f)\,\varepsilon^{I}_{ij} + f\varepsilon^{II}_{ij} \quad (5)$$

The above equations are also applicable to the materials in which the volume fraction of the strong phase is large enough to surround the weak phase, if we assume that the weak second phase is embedded in the strong matrix.

2.2. Analysis of creep deformation [7]

The creep deformation of ductile two-phase alloys at a current time, t, can be calculated on the basis of the continuum mechanics model. If the creep laws for both phases are expressed as arbitrary functions, F^I and F^{II}, of equivalent stresses, σ^I_e and σ^{II}_e, equivalent creep strains, ε^I and ε^{II}, etc., at a current time, t, the increments of equivalent creep strain, $d\varepsilon^I$ and $d\varepsilon^{II}$, during an infinitesimal time interval, dt, are expressed as

$$d\varepsilon^{I} = F^{I}(\sigma^{I}_{e}, \varepsilon^{I}, \ldots)dt \quad (6a)$$

$$d\varepsilon^{II} = F^{II}(\sigma^{II}_{e}, \varepsilon^{II}, \ldots)dt \quad (6b)$$

where the equivalent creep strains at a current time, t, is given by

$$\varepsilon^{I} = \int_{t=0}^{t} d\varepsilon^{I} \quad (7a)$$

$$\varepsilon^{II} = \int_{t=0}^{t} d\varepsilon^{II} \quad (7b)$$

Corresponding increments of creep strains are

$$d\varepsilon^{I}_{ij} = (3\sigma'^{I}_{ij}/2\sigma^{I}_{e})d\varepsilon^{I} \quad (8a)$$

$$d\varepsilon^{II}_{ij} = (3\sigma'^{II}_{ij}/2\sigma^{II}_{e})d\varepsilon^{II} \quad (8b)$$

Using Equations 6–8, the mean creep rate of the two-phase alloy, $\dot{\varepsilon}_{ij}$ ($= d\varepsilon_{ij}/dt$), is given by

$$\dot{\varepsilon}_{ij} = (1-f)(d\varepsilon^{I}_{ij}/dt) + f(d\varepsilon^{II}_{ij}/dt) \quad (s^{-1}) \quad (9)$$

2.3. Constitutive equation

In this study, the Θ projection concept was chosen to express the whole creep curves of both second phase and matrix phase [5]. Creep strain, ε, and creep rate, $\dot{\varepsilon}$, are given by

$$\varepsilon = \theta_1[1 - \exp(-\theta_2 t)] + \theta_3[\exp(\theta_4 t) - 1] \quad (10)$$

$$\dot{\varepsilon} = \theta_1\theta_2 \exp(-\theta_2 t) + \theta_3\theta_4 \exp(\theta_4 t) \ (s^{-1}) \quad (11)$$

$$\log_{10}\theta_i = a_i + b_i T + c_i\sigma + d_i T\sigma \quad (i = 1\text{–}4) \quad (12)$$

where a_i, b_i, c_i and d_i are constants obtained experimentally. T and σ are temperature and stress, respectively. Equation 12 is reduced to the following equation at a constant temperature.

$$\log_{10}\theta_i = A_i + B_i\sigma \quad (i = 1\text{–}4) \quad (13)$$

where A_i and B_i are constants. The creep strain increment, $\Delta\varepsilon$, during a small time interval, Δt ($t \leqslant t \leqslant t + \Delta t$), under a constant stress is expressed as

$$\Delta\varepsilon = \dot{\varepsilon}\Delta t \quad (14)$$

If the interaction of creep deformation between second phase and matrix phase is taken into account, the creep rate at time t is expressed as follows by using Equations 8, 11 and 13

$$\dot{\varepsilon}^{I}_{33} = \theta^{I}_1\theta^{I}_2\exp(-\theta^{I}_2 t) + \theta^{I}_3\theta^{I}_4\exp(\theta^{I}_4 t) \ (s^{-1}) \quad (15a)$$

$$\log_{10}\theta^{I}_i = A^{I}_i + B^{I}_i\sigma^{I}_e = A^{I}_i + B^{I}_i(\sigma^{A}_{33} - fKEx) \quad (i = 1\text{–}4) \quad (15b)$$

for the matrix and

$$\dot{\varepsilon}^{II}_{33} = \theta^{II}_1 \theta^{II}_2 \exp(-\theta^{II}_2 t) + \theta^{II}_3 \theta^{II}_4 \exp(\theta^{II}_4 t) \quad (s^{-1}) \quad (16a)$$

$$\log_{10} \theta^{II}_i = A^{II}_i + B^{II}_i \sigma^{II}_e = A^{II}_i + B^{II}_i [\sigma^{A}_{33} + (1-f)KEx] \quad (i = 1\text{–}4) \quad (16b)$$

for the second phase, where A^{I}_i, B^{I}_i, A^{II}_i and B^{II}_i are constants. The creep rate of the alloy, $\dot{\varepsilon}_{33}$, is given by

$$\dot{\varepsilon}_{33} = (1-f)\dot{\varepsilon}^{I}_{33} + f\dot{\varepsilon}^{II}_{33} \quad (s^{-1}) \quad (17)$$

The creep strain increments in individual phases and the whole material during a small time interval, Δt, are expressed as

$$\Delta\varepsilon^{I}_{33} = \dot{\varepsilon}^{I}_{33}\Delta t \quad (18a)$$

$$\Delta\varepsilon^{II}_{33} = \dot{\varepsilon}^{II}_{33}\Delta t \quad (18b)$$

$$\Delta\varepsilon_{33} = \dot{\varepsilon}_{33}\Delta t \quad (18c)$$

The increment in creep strain difference between two phases, Δx, is expressed as

$$\Delta x = \Delta\varepsilon^{I}_{33} - \Delta\varepsilon^{II}_{33} \quad (19)$$

The value of Δx (and x) is positive when the second phase is stronger than the matrix, and is negative when the former is the weaker phase.

2.4. Calculation of creep curves in ductile two-phase alloys

Creep deformation of two-phase alloys can be calculated by the following procedure on the basis of the continuum mechanics model.

1. The values of $\dot{\varepsilon}^{I}_{33}$ and $\dot{\varepsilon}^{II}_{33}$ are calculated under an initial condition of $\varepsilon^{I}_{ij} = \varepsilon^{II}_{ij} = 0$ at $t = 0$, when a tensile stress, σ^{A}_{33}, is applied (Equations 15 and 16).
2. Strain increments in both phases, $\Delta\varepsilon^{I}_{ij}$ and $\Delta\varepsilon^{II}_{ij}$, and in the alloy, $\Delta\varepsilon_{ij}$, and the increment of strain difference, Δx, are obtained from Equations 15, 16, 18 and 19, provided that the creep rate in each phase is constant during a short time interval, $\Delta t (t \leqslant t \leqslant t + \Delta t)$.
3. Calculated values of these variables are added to those of ε^{I}_{ij}, ε^{II}_{ij}, ε_{ij} and x (at time t), and those values ($\varepsilon^{I}_{ij} + \Delta\varepsilon^{I}_{ij}$, $\varepsilon^{II}_{ij} + \Delta\varepsilon^{II}_{ij}$, $\varepsilon_{ij} + \Delta\varepsilon_{ij}$ and $x + \Delta x$) at the time $t + \Delta t$ are determined.
4. Creep rate in each phase at the time $t + \Delta t$ is calculated on the basis of the creep law (Equations 15 and 16).
5. The procedure from 2 to 4 above is repeated until the creep strain of the two-phase alloy, ε_{33}, reaches the fracture strain.

3. Comparison of calculation results with experimental ones

3.1. Simulation of creep curves by continuum mechanics model

Creep–rupture experiments were carried out using carbon steels of ferrite–pearlite structure with various pearlite volume fractions, f, at 873 K in air. All the creep specimens were solution heated for 3.6 or 7.2 ks in the temperature range 1323–1423 K to obtain almost the same grain size. These specimens were air-cooled to 973 K after solution heating, and then furnace-cooled from 973 K to room temperature to develop various volume fractions of pearlite. The resulting grain size of the specimens was in the range 72–82 μm. Creep curves of ferrite steel (matrix) and pearlite steel (second phase) were simulated by the Θ projection concept. Fig. 1 shows examples of experimental creep curves and simulated ones by the Θ projection concept in a ferrite steel and a pearlite steel at 873 K. The simulated creep curves agree well with the experimental ones in the whole creep deformation process. Figs 2 and 3 show the stress dependence of θ_i parameters in both ferrite and pearlite steels during creep at 873 K when the creep

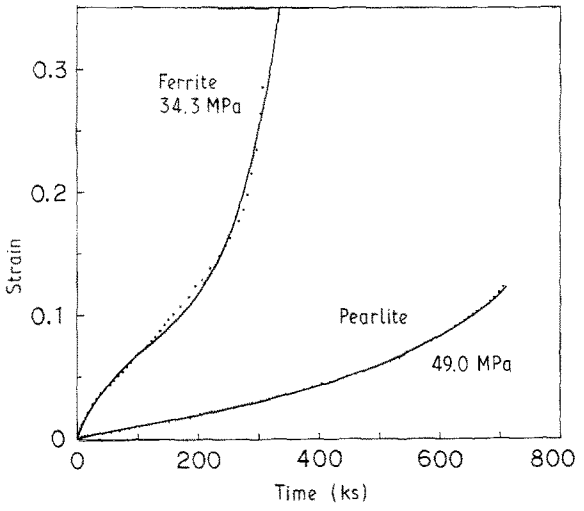

Figure 1 Examples of (. . .) experimental and (——) simulated creep curves by Θ projection concept in both ferrite and pearlite steels at 873 K.

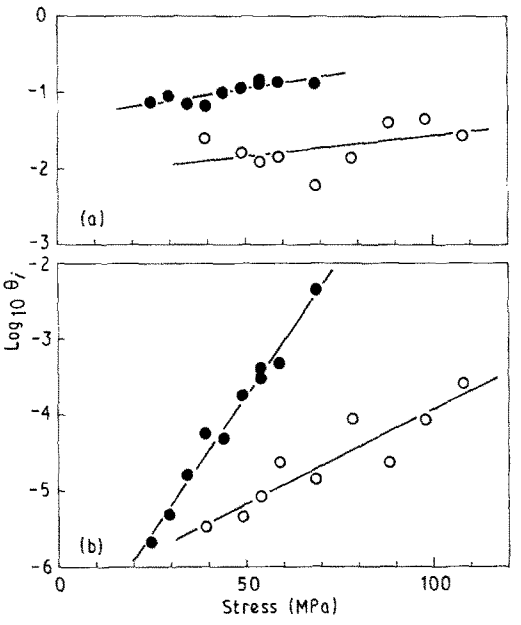

Figure 2 The stress dependence of θ_i parameters (a, θ_1; b, θ_2) in both (●) ferrite and (○) pearlite steels during creep at 873 K.

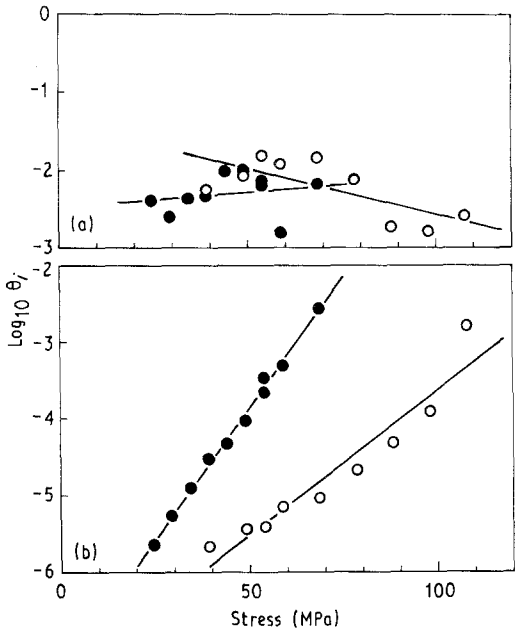

Figure 3 The stress dependence of θ_1 parameters (a, θ_3; b, θ_4) in both (●) ferrite and (○) pearlite steels during creep at 873 K.

curves are simulated by the Θ projection concept. The four θ_i parameters are given by

$$\log_{10}\theta_1^{\mathrm{I}} = -1.344 + 7.889\times10^{-3}\,\sigma_e^{\mathrm{I}} \quad (20a)$$

$$\log_{10}\theta_2^{\mathrm{I}} = -7.342 + 0.07186\,\sigma_e^{\mathrm{I}} \quad (20b)$$

$$\log_{10}\theta_3^{\mathrm{I}} = -2.482 + 4.051\times10^{-3}\,\sigma_e^{\mathrm{I}} \quad (20c)$$

$$\log_{10}\theta_4^{\mathrm{I}} = -7.287 + 0.06841\,\sigma_e^{\mathrm{I}} \quad (20d)$$

for ferrite steels and

$$\log_{10}\theta_1^{\mathrm{II}} = -2.114 + 5.585\times10^{-3}\,\sigma_e^{\mathrm{II}} \quad (21a)$$

$$\log_{10}\theta_2^{\mathrm{II}} = -6.408 + 0.02481\,\sigma_e^{\mathrm{II}} \quad (21b)$$

$$\log_{10}\theta_3^{\mathrm{II}} = -1.386 - 0.01179\,\sigma_e^{\mathrm{II}} \quad (21c)$$

$$\log_{10}\theta_4^{\mathrm{II}} = -7.381 + 0.03744\,\sigma_e^{\mathrm{II}} \quad (21d)$$

for pearlite steels.

Fig. 4 shows the experimental creep curves and the calculated ones based on the continuum mechanics model of ferrite–pearlite steels crept under a stress of 58.8 MPa at 873 K. The physical constants used in the numerical calculations are $E = 1.65\times10^5$ MPa and $\nu = 0.34$ [13], and the shape of the minor phase (pearlite phase in ferrite matrix or ferrite phase in pearlite matrix) is assumed to be spherical. The continuum mechanics model which incorporates the Θ projection concept can explain the change in creep curves with pearlite volume fraction in the experimental results, although the results of the calculations yield somewhat shorter rupture life compared with the experimental ones. Fig. 5 shows the stress dependence of the creep ductility (elongation) in both ferrite and pearlite steels at 873 K. The stress dependence of the elongation, ε_r, is given by

$$\varepsilon_r^{\mathrm{I}} = 0.128\,\sigma^{0.386} \quad (22)$$

for ferrite steels and

$$\varepsilon_r^{\mathrm{II}} = 0.0336\,\sigma^{0.405} \quad (23)$$

for pearlite steels. Therefore, the rule of mixture gives a measure of the rupture ductility in ferrite–pearlite steels, ε_r, such that

$$\varepsilon_r = (1-f)\,\varepsilon_r^{\mathrm{I}} + f\varepsilon_r^{\mathrm{II}} \quad (24)$$

The numerical calculations in Fig. 4 were made up to the elongation estimated by the above equation.

Fig. 6 shows the change in the calculated creep rate with time in the ferrite–pearlite steel with pearlite volume fraction of 0.286 under a stress of 58.8 MPa at 873 K. The simulated creep rate by the Θ projection concept for the ferrite steel and the pearlite steel are also shown in this figure. The creep rate of the ferrite–pearlite steel decreases with time to reach to almost constant creep rate, and increases abruptly after showing a minimum value, while the creep rates of the ferrite steel and the pearlite steel do not exhibit

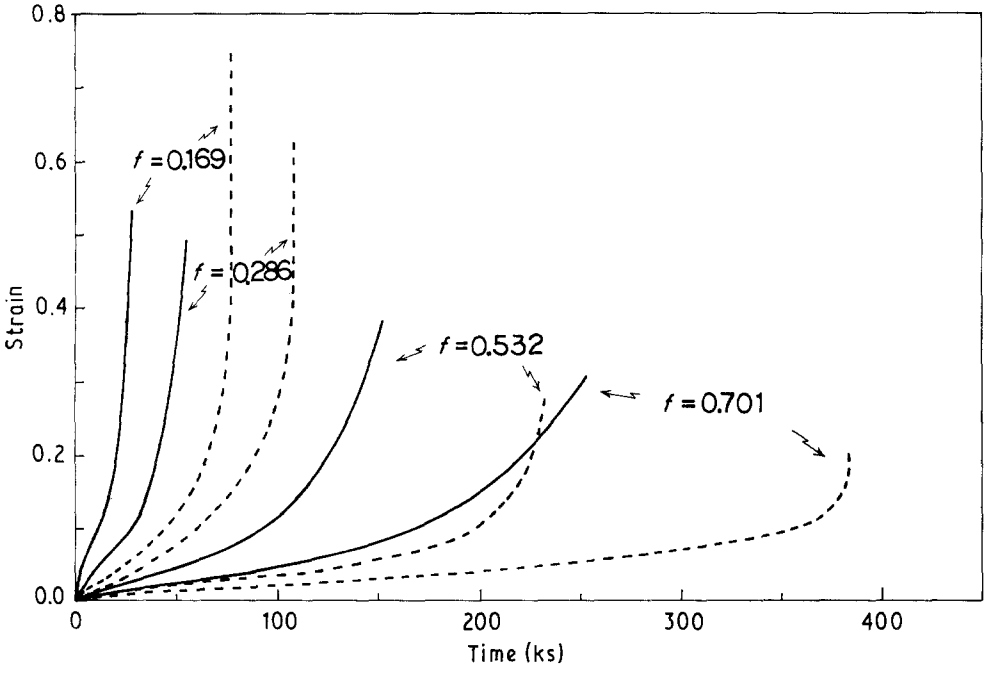

Figure 4 The (– – –) experimental and (——) calculated creep curves based on the continuum mechanics model of ferrite–pearlite steels crept under a stress of 58.8 MPa at 873 K. f = volume fraction of pearlite.

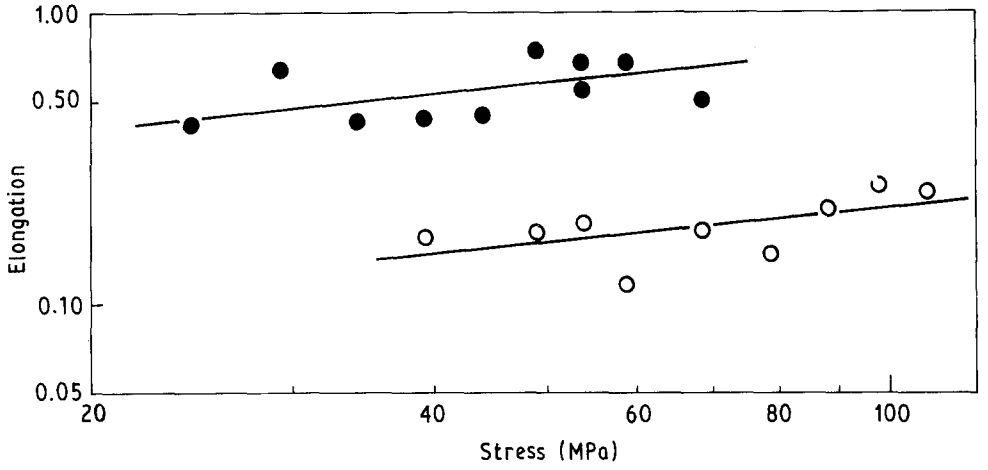

Figure 5 The stress dependence of the creep ductility (elongation) in both (●) ferrite and (○) pearlite steels at 873 K.

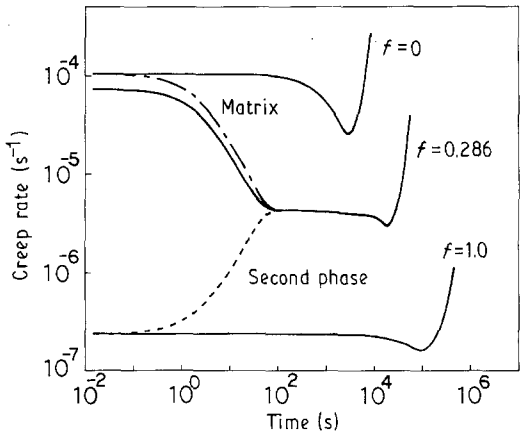

Figure 6 The change in the calculated creep rate with time in a ferrite–pearlite steel with pearlite volume fraction, f, of 0.286 under a stress of 58.8 MPa at 873 K.

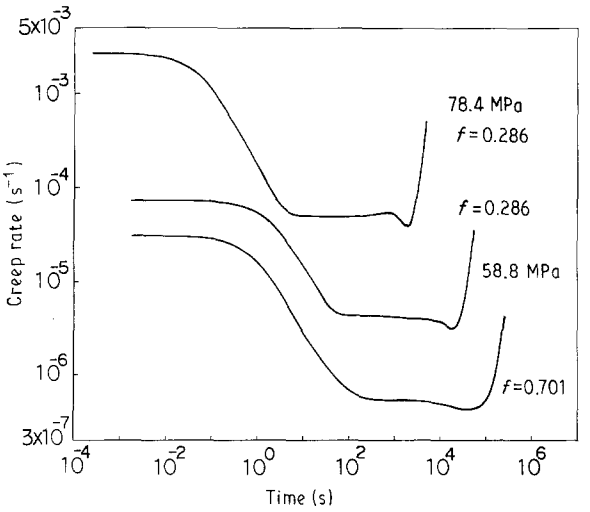

Figure 7 The change in the calculated creep rate with time in the ferrite–pearlite steels during creep at 873 K.

the long steady-state creep. The change in the calculated creep rate is also shown for the ferrite matrix and the pearlite phase of the ferrite–pearlite steel. The creep rate of the ferrite matrix decreases and that of the pearlite phase increases with time to the "steady-state creep" regime, but the creep rates of both phases are the same from the steady-state creep to the rupture. Fig. 7 shows the change in the calculated creep rate with time in the ferrite–pearlite steels during creep at 873 K. As shown in this figure, the calculated creep rate of the ferrite–pearlite steels with various volume fraction of pearlite exhibited the steady-state creep regime under different creep stresses.

Fig. 8 shows the change in the creep rate with time in a ferrite steel, a pearlite steel and a ferrite–pearlite steel (pearlite volume fraction, $f = 0.286$) under a stress of 58.8 MPa at 873 K. The experimental results indicate that the ferrite–pearlite steel clearly exhibits the steady-state creep regime, while both the ferrite steel and the pearlite steel do not have a long steady-state creep. Fig. 9 shows the change in the creep rate with time in ferrite–pearlite steels at 873 K. The steady-state creep regime was also observed in the specimens with various pearlite volume fractions under different creep stresses. Thus, the results of the calculations (Figs 6 and 7) agree with the experimental

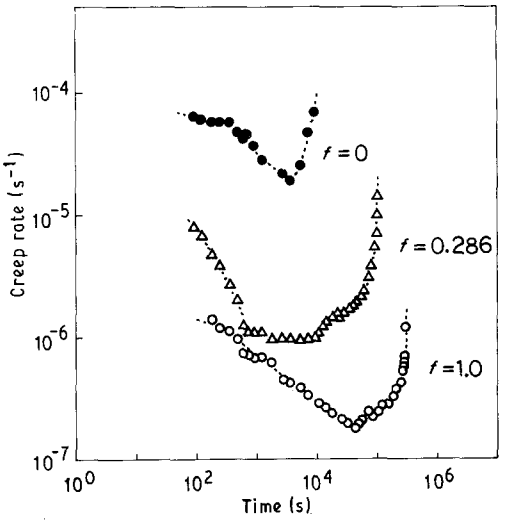

Figure 8 The change in the creep rate with time in a ferrite steel, a pearlite steel and a ferrite–pearlite steel (pearlite volume fraction, $f = 0.286$) under a stress of 58.8 MPa at 873 K.

results shown in Figs 8 and 9. It is interesting to note that two-phase alloys exhibit a "steady-state creep", even if both second phase and matrix do not have inherent steady-state creep.

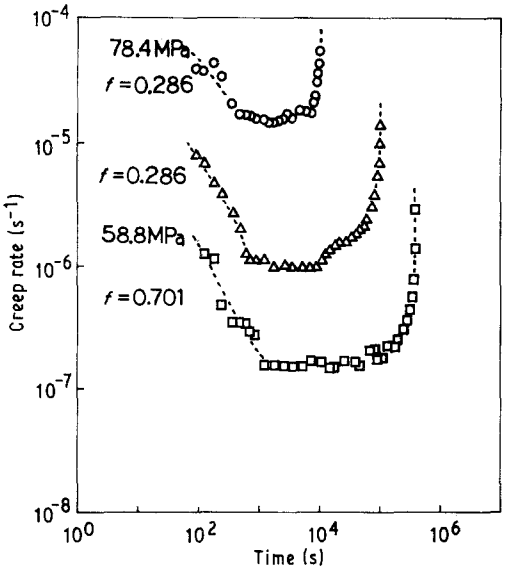

Figure 9 The change in the creep rate with time in ferrite–pearlite steels at 873 K.

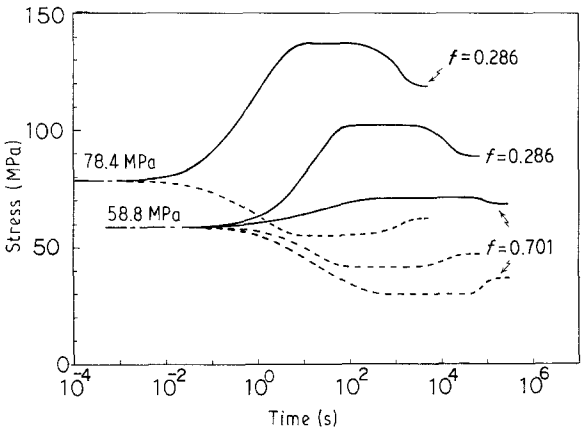

Figure 10 The change in the equivalent stresses of the ferrite matrix and the pearlite phase in the ferrite–pearlite steels during creep at 873 K. (– – –) σ_e^I, (——) σ_e^{II}.

Fig. 10 shows the change in the equivalent stresses of the ferrite matrix and the pearlite phase during creep at 873 K. The equivalent stress of the ferrite matrix, σ_e^I, decreases and that of the pearlite phase, σ_e^{II}, increases with time and reaches to the steady-state values. The equivalent stress of the ferrite matrix increases and that of the pearlite phase decreases with time after the steady state. The difference in the equivalent stresses between two phases is larger in the steel with the smaller pearlite volume fraction ($f = 0.286$) under the same creep stress, and it is larger in the same steel under the higher creep stress (78.4 MPa). As shown in these figures, the steady-state creep is caused by the internal stresses in both second phase and matrix arising from the strength difference between these two phases.

3.2. Life prediction by continuum mechanics model

The continuum mechanics model in this study is applicable to the rupture life prediction of two-phase alloys by using the creep data of two phases which constitute the two-phase alloys. Fig. 11 shows the experimental rupture life and the calculated one in the ferrite–pearlite steels crept at 873 K. The calculated rupture life was estimated on the basis of the continuum mechanics model which incorporates the Θ projection concept. The calculated rupture life was obtained as the time when the calculated creep strain reached to the rupture ductility (elongation) defined by Equation 24. The results of the calculations are correlated well with the experimental results, although the analytical results give somewhat shorter rupture life, especially under the lower stresses. Thus, the rupture life of two-phase alloys can be predicted by the continuum mechanics model from the existing creep data of the individual phases which constitute the two-phase alloys, although the continuum mechanics model does not take into account the fracture process, such as the initiation and growth of cracks.

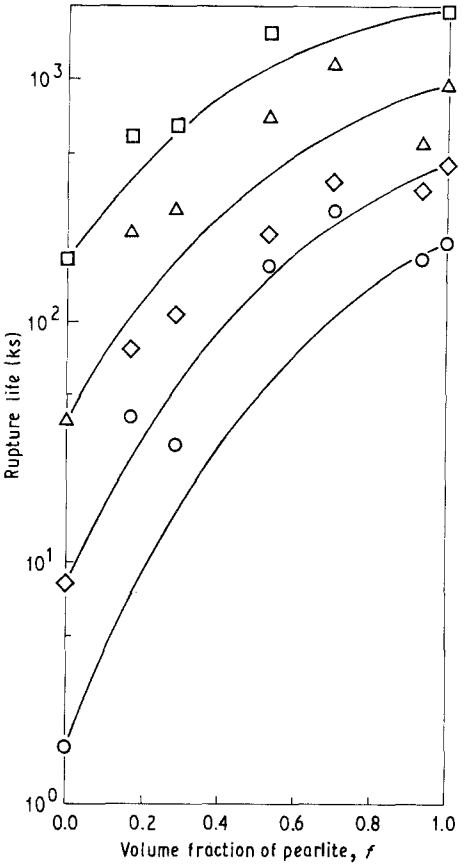

Figure 11 The experimental and calculated rupture life in the ferrite–pearlite steels crept at 873 K. Stress (MPa): (□) 39.2, (△) 49.0, (◇) 58.8, (○) 68.6, (——) calculated.

The continuum mechanics model in this study can simulate the whole creep deformation process of the ductile two-phase alloys from the onset of creep loading to the final rupture. Therefore, the continuum mechanics model is also applicable not only to the life prediction but also to the creep–strength design of the ductile two-phase alloys.

4. Conclusions

The creep deformation of the ductile two-phase alloys was analysed on the basis of the continuum mechanics

model which incorporated the Θ projection concept proposed by Evans and Wilshire. The calculation results were compared with the experimental ones in ferrite–pearlite steels. The results obtained were summarized as follows.

1. The continuum mechanics model was able to predict the whole creep deformation process of the ductile two-phase alloys from the onset of creep loading to the final rupture from the existing creep data of the individual phases which constituted the two-phase alloys. The analytical results based on the present model correlated well with the experimental results in ferrite–pearlite steels.

2. A "steady-state creep" in the ductile two-phase alloys was predicted by the continuum mechanics model, even if the constituent phases did not have the inherent steady-state creep. The creep rate of the ductile two-phase alloys decreased with time to the steady state, and then increased abruptly to the final rupture. This was caused by the internal stresses arising from the creep–strength difference between two phases in the two-phase alloys. This steady-state creep was observed in ferrite–pearlite steels during creep at 873 K.

3. The continuum mechanics model revealed that in the ductile two-phase alloys the creep rate of the ferrite matrix decreased and that of the pearlite (second) phase increased with time to a certain value of the steady-state creep rate. The model also showed that the creep rate of the matrix was the same as that of the second phase from the steady-state creep to the final rupture.

4. The predicted rupture life on the basis of the continuum mechanics model agreed well with the experimental results in ferrite–pearlite steels under higher stresses, although the exact fracture process of the alloys was not taken into account in the present model. The continuum mechanics model was able to apply to the life prediction and the creep–strength design of the ductile two-phase alloys.

Acknowledgement

The author thanks Nippon Steel Corporation for supplying the carbon steels used in this study.

References

1. A. H. SULLY, "Metallic Creep and Creep Resistant Alloys" (Butterworths Scientific, London, 1949) p. 37.
2. F. K. G. ODQVIST and J. HULT, "Kriechfestigkeit Metallischer Werkstoffe", translated by S. Murakami (Baifukan, Tokyo, 1967) p. 73.
3. F. GAROFALO, "Fundamentals of Creep and Creep–Rupture in Metals", translated by M. Adachi, (Maruzen, Tokyo, 1968) p. 10.
4. V. LUPINC, in "Creep and Fatigue in High Temperature Alloys", edited by J. Bressers (Applied Science, London, 1981) p. 7.
5. R. W. EVANS and B. WILSHIRE, "Creep of Metals and Alloys" (The Institute of Metals, London, 1985) p. 189.
6. R. W. EVANS, P. J. SCHARNING and B. WILSHIRE, in "Creep Behaviour of Crystalline Solids", edited by B. Wilshire and R. W. Evans (Pineridge Press, Swansea, 1985) p. 201.
7. M. TANAKA, T. SAKAKI and H. IIZUKA, *Acta Metall. Mater.* **39** (1991) 1549.
8. J. D. ESHELBY, *Proc. R. Soc.*, **A241** (1957) 376.
9. T. MURA and T. MORI, "Micromechanics" (Baifukan, Tokyo, 1976) p. 23.
10. T. MURA, "Micromechanics of Defects in Solids" (Martinus Nijhoff, The Hague, 1982) p. 63.
11. T. MORI and K. TANAKA, *Acta Metall.* **21** (1973) 571.
12. K. TANAKA and T. MORI, *ibid.* **18** (1970) 931.
13. Technical Data, "Elastic Moduli of Metallic Materials", (Japan Society of Mechanical Engineers, Tokyo, 1980) p. 137.

Received 2 January
and accepted 29 October 1992